Quantum Electronics **38** (1) 16 – 22 (2008)

LASERS

PACS numbers: 42.55.Px; 42.55.Sa; 42.60.Da
DOI: 10.1070/QE2008v038n01ABEH013633

Modes of a semiconductor rectangular microcavity

D.V. Batrak, A.P. Bogatov, A.E. Drakin, N.V. D'yachkov, D.R. Miftakhutdinov

***Abstract*. The mode parameters of a rectangular cavity of a semiconductor laser emitting in the range from 850 to 880 nm are numerically calculated and analysed. Nearly quadratic microcavities with a side of length $\sim$10 μm are considered. It is shown that, unlike a Fabry – Perot cavity, a rectangular cavity has a much more dense system of nonequidistant modes, which in principle cannot be interpreted as modes of an 'efficient' Fabry – Perot cavity or a ring cavity. The maximum Q factor of modes in the cavities under study can exceed 10^5, which corresponds to the reduced intracavity loss $\sim$3 cm^{-1}. The radiation field of the cavity can be interpreted as the field of four coherent sources located at the cavity corners.**

Keywords: *semiconductor rectangular cavity, mode Q factor.*

1. Introduction

Dielectric cavities for optical fields corresponding to the waves propagating along closed trajectories and experiencing total internal reflection from the cavity boundaries occupy a special place among optical cavities of all other types. This is explained by their comparatively high Q factor along with a comparatively small size. The most spectacular representatives of such cavities are, for example, spherical microcavities (see [1 – 3] and references therein). Another widespread configuration of such cavities is rectangular semiconductor structures [4 – 6].

These cavities attract interest mainly because they can be used as small narrowband optical filters. Nevertheless, studies were reported in which such cavities containing an amplifying medium were used in lasers. One of the first studies of lasers with a spherical cavity was performed in [7]. The earlier studies of semiconductor lasers were performed for rectangular cavities.

However, rectangular cavities were widely used in semiconductor lasers only at the initial stage of their development; later, interest in these lasers was virtually lost because of their low efficiency. A rectangular cavity is fabricated in a simplified way by the face cleavage. The threshold lasing current of such a laser virtually coincides with the transparency threshold of a heterostructure due to a high Q factor of its cavity. At present rectangular cavity lasers are mainly used to test rapidly the emission properties of heterostructures at the intermediate stage of fabrication of lasers from them. The mode structure of the cavity is not important for such applications and is not considered, as a rule. It seems that for this reason, as far as we know, the mode spectrum of a rectangular cavity of a semiconductor laser has not been investigated in detail so far.

Nevertheless, it would be premature to exclude the possibility of other than technological applications of rectangular cavity lasers. In particular, they can be used in cases when the main characteristic is radiation coherence rather than the output power, for example, as probe oscillators, for optical heterodyning, etc.

In connection with the mode structure of the spectrum of such lasers, it is pertinent to point out papers [8, 9] in which the unproved analysis of the mode structure of a rectangular (square) cavity was performed in terms of an equivalent Fabry – Perot cavity with an efficient length, which was larger by a factor of $\sqrt{2}$ than the cavity side. Based on his analysis, the author of papers [8, 9] made a conclusion that an active semiconductor medium possesses 'the self-induced supertransparency'. In this connection we believe that it is necessary to study resonances of a rectangular cavity of a semiconductor laser more consistently and in more detail. Earlier papers [5, 6] report the results of numerical calculations of the mode spectrum of a rectangular cavity, but parameters used in these papers and the neglect of the refractive index dispersion complicate the application of these results for analysis of a rectangular cavity of a semiconductor laser with typical parameters. The aim of our paper is to calculate and analyse the mode spectrum of a rectangular cavity of a semiconductor laser similar to that used in [8, 9] and emitting in the spectral range from 850 to 880 nm. We considered first of all nearly square microcavities with a square side of $\sim$10 μm. Such cavities are not too small yet and can be easily fabricated, but at the same time they are too large for their mode spectrum to be quasi-continuous.

2. Calculation of frequencies and mode Q factors

We calculate a heterostructure consisting of layers in the plane xy with refractive indices providing the propagation

D.V. Batrak, A.P. Bogatov, A.E. Drakin, N.V. D'yachkov, D.R. Miftakhutdinov P.N. Lebedev Physics Institute, Russian Academy of Sciences, Leninsky prosp. 53, 119991 Moscow, Russia;
e-mail: bogatov@sci.lebedev.ru

Received 22 May 2007
Kvantovaya Elektronika **38** (1) 16 – 22 (2008)
Translated by M.N. Sapozhnikov

of the TE and TM waves whose field $h(z)\exp(\mathrm{i}k_x x + \mathrm{i}k_y y - \mathrm{i}\omega t)$ admits the separation of variables. The electromagnetic field of these waves can be completely described by considering only the magnetic field amplitude (H_z for the TE modes) or the electric field amplitude (E_z for the TM modes) and the two-dimensional wave vector $\boldsymbol{k}$ whose modulus is related to the frequency through the effective refractive index $|\boldsymbol{k}| = n\omega/c$ (hereafter, simply 'refractive index'). In the general case a monochromatic field in such a structure can be represented in the form of a superposition of such waves as $h(z)F(x,y)\exp(-\mathrm{i}\omega t)$. The function $F(x,y)$ is normalised so that the maximum of its modulus is equal to unity. The refractive index in our calculations has a linear dispersion $n(\lambda) = n(\lambda_0) + \partial n/\partial\lambda|_{\lambda=\lambda_0}(\lambda - \lambda_0)$, where $\lambda = c/\omega$. If the structure size is not limited along the x axis and limited along the y axis ($|y| < b/2$), the exact solution of Maxwell's equations gives modes for a waveguide formed by the jump in the refractive index at the boundaries $y = \pm b/2$. The field

$$F(x,y) = [C_1\exp(\mathrm{i}k_x x) + C_2\exp(-\mathrm{i}k_x x)]u(y)$$

of these modes is formed by the two waves counter-propagating along the x axis. The amplitude of the waves is described by the expressions

$$u(y) = \begin{cases} \cos(k_y y - \phi_y), & |y| \leqslant b/2, \\ \cos(k_y b/2 - \phi_y)\exp[-\gamma_y(y - b/2)], & y > b/2, \\ \cos(-k_y b/2 - \phi_y)\exp[\gamma_y(y + b/2)], & y < -b/2. \end{cases}$$

Here, $k_x^2 + k_y^2 = n^2 k_0^2$; $k_x^2 - \gamma_y^2 = k_0^2$; $\tan[\frac{1}{2}(k_y b - \pi m)] = \eta\gamma_y/k_y$; C_1 and C_2 are arbitrary constants, which are determined in principle by the conditions for $x = \pm\infty$; $k_0 = \omega/c$ is the wave vector modulus in vacuum; m is the mode index; $\phi_y = 0$ and $\pi/2$ for even and odd m, respectively; $\eta = n^2$ and 1 for the TE and TM modes, respectively. Figure 1a shows schematically the propagation of these waves.

The exact solution for a structure unlimited along the y axis and limited along the x axis ($|x| < a/2$, Fig. 1b) can be found similarly. The field of modes in such a waveguide has the form

$$F(x,y) = [C_3\exp(\mathrm{i}k_y y) + C_4\exp(-\mathrm{i}k_y y)]v(x).$$

The amplitude of the waves is

$$v(x) = \begin{cases} \cos(k_x x - \phi_x), & |x| \leqslant a/2, \\ \cos(k_x a/2 - \phi_x)\exp[-\gamma_x(x - a/2)], & x > a/2, \\ \cos(-k_x a/2 - \phi_x)\exp[\gamma_x(x + a/2)], & x < -a/2. \end{cases}$$

Here, $k_x^2 + k_y^2 = n^2 k_0^2$; $k_y^2 - \gamma_x^2 = k_0^2$; $\tan[\frac{1}{2}(k_x a - \pi n)] = \eta\gamma_x/k_x$; n is the mode index; $\phi_x = 0$ and $\pi/2$ for even and odd n, respectively.

Now we can compose from these two exact solutions the approximate solution for the structure in Fig. 1c limited along the x and y axes ($|x| < a/2$ and $|y| < b/2$) and corresponding to a rectangular cavity. For this purpose, by using the boundary conditions for $x = \pm a/2$ and $y = \pm b/2$, we find the coefficients $C_1 \div C_4$. As a result, we obtain the field $F(x,y)$ in the cavity:

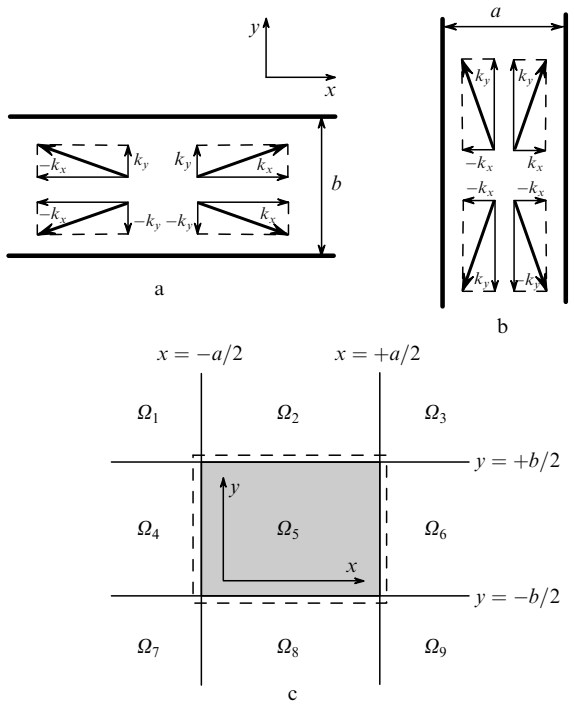

Figure 1. Schematic representation of the formation of a rectangular two-dimensional waveguide (c) from two one-dimensional waveguides (a, b); Ω_i $(i = 1-9)$ are different regions of the two-dimensional waveguide.

$$F(x,y) = \begin{cases} \cos(k_x x - \phi_x)\cos(k_y y - \phi_y), & |x| \leqslant a/2, \ |y| \leqslant b/2, \\ \cos(k_x a/2 - \phi_x)\cos(k_y y - \phi_y)\exp[-\gamma_x(x - a/2)], & x > a/2, \ |y| < b/2, \\ \cos(-k_x a/2 - \phi_x)\cos(k_y y - \phi_y)\exp[\gamma_x(x + a/2)], & x < -a/2, \ |y| < b/2, \\ \cos(-k_x x - \phi_x)\cos(k_y b/2 - \phi_y)\exp[-\gamma_y(y - b/2)], & |x| < a/2, \ y > b/2, \\ \cos(k_x x - \phi_x)\cos(-k_y b/2 - \phi_y)\exp[\gamma_y(y + b/2)], & |x| < -a/2, \ y < -b/2, \\ 0, & |x| > a/2, |y| > b/2, \end{cases} \quad (1)$$

where $k_x^2 + k_y^2 = n^2 k_0^2$; $k_x^2 - \gamma_y^2 = k_0^2$; $k_y^2 - \gamma_x^2 = k_0^2$; $k_x\tan(\frac{1}{2}k_x a - \phi_x) = \eta\gamma_x$; $k_y\tan(\frac{1}{2}k_y b - \phi_y) = \eta\gamma$; the values of $\phi_{x,y}$ are equal to 0 or $\pi/2$ for the even or odd mode index, respectively, in the direction of x or y (the mode index is equal, as usual, to the number of zeroes of the distribution function); and $\eta = 1$ and n^2 for the TM and TE modes, respectively. Such an approach corresponds to the Marcatili analysis of a rectangular dielectric waveguide [10].

The system of equations (1) was earlier used in papers [5, 6] to calculate a square cavity with a side of ~ 2 μm and the refractive index $n \approx 3$. Despite its intricate form, system (1) can be easily solved numerically. Figure 2 shows one of the field intensity distributions near the corner of a cavity of size 13×14.

The obtained solution is not exact because it is not defined, in particular, in regions Ω_i (Fig. 1c) for $i = 1, 3, 7, 9$. But if the characteristic size of the cavity is large enough compared to the wavelength in the medium and the modes under study are located far away from the cut-off mode, we can assume that the field energy in regions Ω_i for $i = 1, 3, 7, 9$ is small compared to that in regions Ω_i for $i = 2, 4, 5, 6, 8$ where Maxwell's equation are fulfilled exactly. In this case, the estimate of the relative measurement error of cavity mode frequencies and Q factors by using the perturbation theory [11] shows that it is insignificant for our problem.

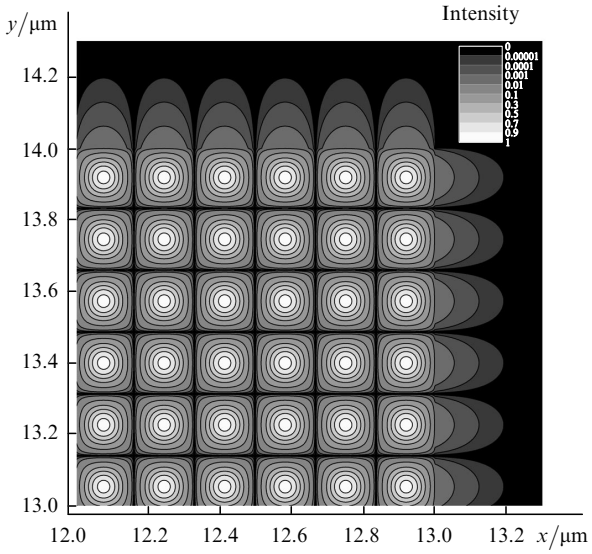

Figure 2. Field intensity distribution $|F(x,y)|^2$ corresponding to the approximate solution near one of the corners of the 13×14-μm cavity; the wavelength is 867.34 nm, the mode indices are $m_x = 76$ and $m_y = 80$.

These considerations are also confirmed by the results obtained in paper [5] in which the solutions of system (1) were compared with the solutions of Maxwell's equations obtained by the direct numerical FDTD method in the entire plane x, y for less favourable conditions due to a considerable smaller size of the cavity ($a = b \sim 2$ μm).

Modes of the type under study can be interpreted as standing waves caused by the closed motion of plane waves which experience total internal reflection from the cavity boundaries. Such waves are characterised by the propagation angle ϕ (for example, with respect to the x axis: $\tan\phi = k_y/k_x$) falling into the region of angles of total internal reflection from faces $x = \pm a/2$ ($\sin\phi < 1/n$) and faces $y = \pm b/2$ ($\cos\phi < 1/n$).

Equations (1) were solved numerically for each pair of indices, thereby determining the frequency of this mode. We considered only modes falling into the typical amplification range of semiconductors emitting in the range from 850 to 880 nm. The Q factors of these modes were determined by calculating the radiation loss by neglecting, for example, scattering losses and intracavity absorption. The far-zone field can be obtained from the field and its normal derivative at some contour:

$$F(r,\phi) = \frac{\exp[\mathrm{i}(k_0 r - 3\pi/4)]}{\sqrt{8\pi k_0 r}} \times \oint_C \exp[-\mathrm{i}k_0(\boldsymbol{\rho},\boldsymbol{e})]\left[\frac{\partial F(\boldsymbol{\rho})}{\partial \boldsymbol{n}} + \mathrm{i}k_0(\boldsymbol{n},\boldsymbol{e})F(\boldsymbol{\rho})\right]\mathrm{d}l, \quad (2)$$

where $\boldsymbol{e}$ is the unit vector in the direction ϕ; C is the integration contour (shown by the dashed contour in Fig. 1c); $\boldsymbol{n}$ is the normal to its contour and $\boldsymbol{\rho}$ is the integration variable. Now the emitted power is

$$P = \int_0^{2\pi} \frac{c}{4\pi}|F(r,\phi)|^2 r\mathrm{d}\phi,$$

and the energy stored in the cavity is

$$W = \frac{n^2}{\eta}\int\int \frac{1 + n_g/n}{8\pi}|F|^2\mathrm{d}x\mathrm{d}y,$$

where n_g is the group refractive index. The mode Q factor is determined from the quantities obtained above:

$$Q = 2\pi\frac{W}{PT} = \omega\frac{W}{P},$$

where T is the oscillation period and ω is the mode frequency. Note, however, that such a definition of the Q factor is not correct in a particular case of a square cavity where even higher Q modes exist, representing a superposition of two frequency-degenerate modes with certain coefficients [6].

3. Radiation field of modes

Let us now find from the far-zone field of modes [integral in (2)] the effective sources producing this field. The amplitude $F(\boldsymbol{R})$ of the far-zone field produced by sources $A(\boldsymbol{r})$ can be written in the form

$$F(\boldsymbol{R}) \sim \int A(\boldsymbol{r})\frac{\exp(\mathrm{i}k|\boldsymbol{R}-\boldsymbol{r}|)}{\sqrt{|\boldsymbol{R}-\boldsymbol{r}|}}\mathrm{d}^2 r \sim \frac{1}{\sqrt{R}}\int A(\boldsymbol{r})\exp(\mathrm{i}k|\boldsymbol{R}-\boldsymbol{r}|)\mathrm{d}^2\boldsymbol{r},$$

where $\boldsymbol{R}$ and $\boldsymbol{r}$ are coordinates in the far and near (in the region of sources) zones, respectively. By expanding the exponential as a power series in $\boldsymbol{r}/\boldsymbol{R}$, we obtain

$$F(\boldsymbol{R}) \sim \frac{\exp(\mathrm{i}kR)}{\sqrt{R}}\int A(\boldsymbol{r})\exp(-\mathrm{i}kr\cos\theta)\mathrm{d}^2 r = \frac{\exp(\mathrm{i}kR)}{\sqrt{R}}K(\phi),$$

where θ is the angle between vectors $\boldsymbol{r}$ and $\boldsymbol{R}$, and the angle ϕ determines the direction of the vector $\boldsymbol{R}$. Let us now pass to the Cartesian coordinates:

$$K(\phi) \sim \int A(x,y)\exp[-\mathrm{i}k(x\cos\phi + y\sin\phi)]\mathrm{d}x\mathrm{d}y.$$

To solve the problem formulated above, we should find the inverse transformation. Consider the transformation

$$\tilde{A}(x,y) = \int K(\phi)\exp[\mathrm{i}k(x\cos\phi + y\sin\phi)]\mathrm{d}\phi. \quad (3)$$

The function $\tilde{A}(x,y)$ is related to the required source function $A(x,y)$ by the expression

$$\tilde{A}(x,y) = \int M(x,y,x',y')A(x',y')\mathrm{d}x'\mathrm{d}y',$$

which is a convolution with the kernel

$$M(x,y,x',y') = \int_0^{2\pi}\exp\{\mathrm{i}k[(x-x')\cos\phi + (y-y')\sin\phi]\}\mathrm{d}\phi = 2\pi J_0(kr),$$

where $r = [(x-x')^2 + (y-y')^2]^{1/2}$. One can see that

transformation (3) solves the formulated problem accurate to a convolution with the Bessel function with the characteristic width of the order of the wavelength.

The visible image of the operating laser can be also interpreted by using the theory of an ideal microscope with a finite aperture for the case of coherent illumination, which was considered, for example, in book [12]. According to this theory, the field in the image plane in the two-dimensional case is expressed in terms of the field in the object plane as

$$F(y') = \int U(\xi) \exp\left(-\mathrm{i}k_0 \frac{y'}{D}\right) \mathrm{d}\xi$$

$$\sim \iint F(y) \exp\left(-\mathrm{i}k_0 \frac{\xi}{f} y\right) \exp\left(\mathrm{i}k_0 \frac{-y'}{D}\right) \mathrm{d}y \mathrm{d}\xi,$$

where ξ changes from $-\mathrm{NA}\, f$ to $+\mathrm{NA}\, f$ (NA is the numerical aperture of the microscope); y and y' are coordinates in the object and image planes, respectively; and f is the focal distance of the microscope objective. The obtained expression can be written in the form

$$F(Y) \sim \int F(y) \frac{\sin[k_0 \mathrm{NA}(Y-y)]}{Y-y} \mathrm{d}y, \qquad (4)$$

where $Y = -y'f/D$.

The function $F(Y)$ determines the field configuration in the image plane of the microscope recalculated to the unit magnification. The square of the modulus of this function gives the image of the cavity in the microscope adjusted to the given object plane. As the object plane, a plane lying between the cavity and microscope should be chosen, because the theory assumes that the space between the object plane and microscope objective is homogeneous. Note also that because the object size is small, the microscope aperture NA should be of the order of unity to obtain a detailed image. The depth of focus of the microscope in the case of such an aperture is measured by several wavelengths, and therefore the object plane should be drawn at a small distance of the order of a wavelength from the cavity boundary. To solve the formulated problem, we should find the field in this plane. Due to the conditions considered above, expression (2) determining the far-zone field cannot be used for this purpose. However, we can use the exact Kirchhoff expression for the two-dimensional case, which describes the propagation of waves in a free space:

$$F(x,y) = \frac{\mathrm{i}}{4} \oint_C \left[F(x_0, y_0) \frac{\partial H_0^{(1)}\{k_0[(x-x_0)^2 + (y-y_0)^2]^{1/2}\}}{\partial \boldsymbol{n}} \right.$$

$$\left. - H_0^{(1)}\{k_0[(x-x_0)^2 + (y-y_0)2]^{1/2}\} \frac{\partial F(x_0 y_0)}{\partial \boldsymbol{n}} \right] \mathrm{d}l. \qquad (5)$$

Here, $H_0^{(1)}(r)$ is the first-order Hankel function of the first kind; x_0 and y_0 are coordinates of a current point on the cavity boundary (C is the integration contour shown by the dashed curve in Fig. 1c); x, y are coordinates of a spatial point at which we seek the field (in our case, this is a straight line in the object plane of the microscope); and $\boldsymbol{n}$ is the external normal to the cavity boundary at the current point. Thus, by calculating from (5) the field on a straight line lying in the object plane of the microscope and not intersecting the cavity boundary and taking then the square of the field in the image plane calculated by expression (4), we can obtain the configuration of the visible image of the cavity.

4. Results

We used in all calculations the values of the refractive index $n = 3.6$ and the group refractive index $n_g = 4.8$ at a central wavelength of 0.86 μm. Dispersion over the entire spectral region of calculations was assumed linear. Figure 3 shows the dependences of mode wavelengths on the angle ϕ ($\tan\phi = k_y/k_x$) for cavities of size 13×13 and 13×14 μm. The curves resembling parabolas corresponds to the modes with a constant sum of indices $m_x + m_y = \mathrm{const}$. One can easily see that modes, especially near the tops of these curves, are located very densely (the intermode distance is $\sim$0.1 nm). The distance between the maxima of the curves corresponds to that for a Fabry–Perot resonator of length equal to the resonator diagonal; however, the entire system of nonequidistant modes cannot be treated as the system of modes of some equivalent Fabry–Perot resonator. In the case of a square cavity, the double frequency degeneracy of modes is observed, which corresponds to the symmetry of coordinates x and y.

Figure 4 shows the Q factors of these modes for a cavity of size 13×14 μm as functions of the propagation angle. The TE modes propagating approximately along the cavity diagonal have the highest Q factor. One can see that the Q factor of modes can exceed 10^5, which corresponds to the reduced intracavity volume loss $\sim 3\ \mathrm{cm}^{-1}$.

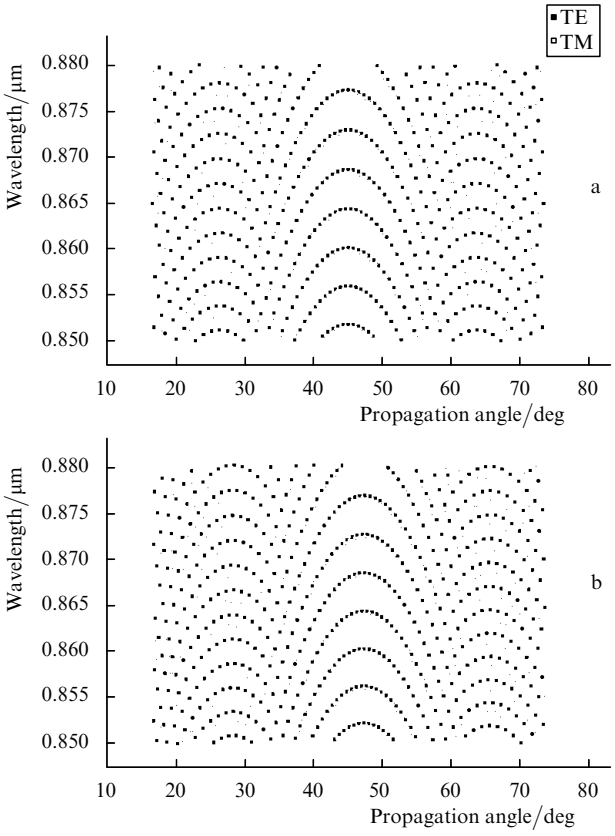

Figure 3. Wavelengths and the propagation angles of modes lying in the interval 0.85 μm $< \lambda <$ 0.88 μm for cavities of sizes 13×13 μm (a) and 13×14 μm (b).

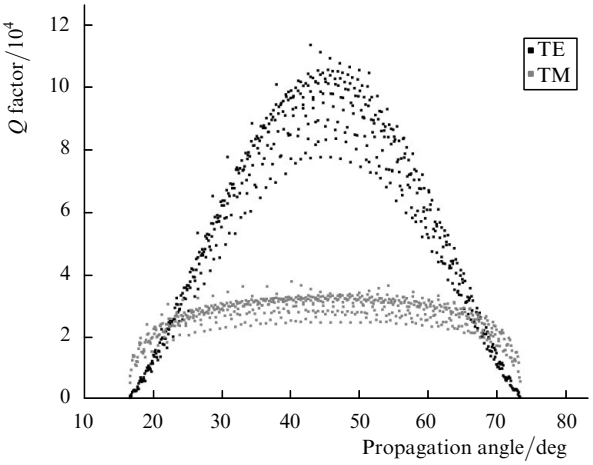

Figure 4. Dependences of the Q factor of modes lying in the interval 0.85 μm $< \lambda <$ 0.88 μm on the propagation angle for the13 × 14-μm cavity.

Figure 5 shows the dependences of the Q factor and mode wavelengths on the cavity size. Figure 5d for a 13 × 13-μm cavity corresponds to the limiting case. By comparing the data presented in Figs 5d and 5a-c, we can see how the double degeneracy of the modes occurs in passing from a rectangular to square cavity.

Table 1 presents the highest-Q modes for different branches shown in Fig. 5.

Figure 6 shows the far field of the mode with indices 76 and 80 along coordinates x and y, respectively, for the 13 × 14 cavity and the far field produced by four coherent sources of the same intensity with the same wavelength located at the corners of a rectangle of the same size. The similarity of these far fields can be interpreted as if the microcavity emits from its corners. This is confirmed by Fig. 7 presenting the intensity distribution $|\tilde{A}(x,y)|^2$ of sources corresponding to the far field of this mode calculated for the given cavity from expression (3).

Figures 8 and 9 present calculated images produced in a microscope by the output radiation of the microcavity. The numerical aperture used in calculations was NA = 0.5. The object plane was assumed to be located at a distance of d (in micrometers) from the cavity boundary and turned around the nearest angle with respect to the y axis through the angle

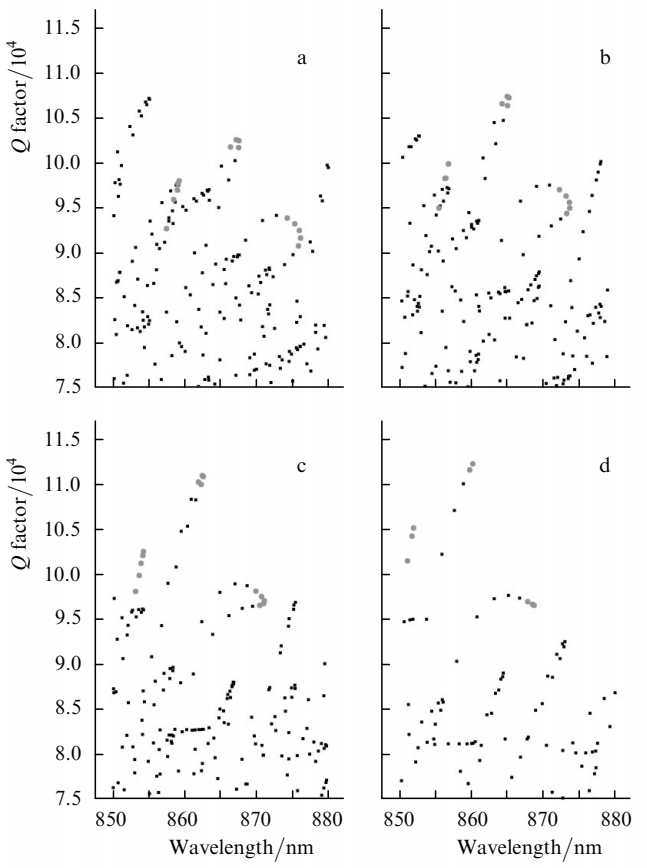

Figure 5. Q factors of different modes for cavities of sizes 13 × 14 (a), 13 × 13.2 (b), 13 × 13.1 (c), and 13 × 13 μm (d).

α. The coordinate origin in the object plane was selected in the following way: if the object plane is parallel to one of the coordinate axes (the angle α is a multiple of 90°), the coordinate origin coincides with the origin of the corresponding axis; if the angle α is not a multiple of 90°, the coordinate origin corresponds to a point nearest to the cavity corner. The corresponding axis is directed to the right when looking at the plane from the cavity centre. Figure 7 shows that the intensity distribution has distinct peaks corresponding to the cavity corners.

Table 1. Q factors of some highest-Q-factor modes of nearly square cavities.

Indices ($m_x + m_y$)	13 × 13.3 μm		13 × 13.2 μm		13 × 13.1 μm		13 × 13 μm	
	λ/nm	$Q/10^5$	λ/nm	$Q/10^5$	λ/nm	$Q/10^5$	λ/nm	$Q/10^5$
73 + 81 = 154	858.96	0.968	856.33	0.981	853.66	0.998	850.96	1.014
75 + 79 = 154	859.22	0.979	856.71	0.997	854.17	1.020	851.59	1.041
77 + 77 = 154	859.05	0.975	856.67	0.997	854.25	1.024	851.80	1.050
79 + 75 = 154	858.47	0.958	856.21	0.981	853.92	1.011	851.59	1.041
81 + 73 = 154	857.46	0.926	854.04	0.900	853.16	0.980	850.96	1.014
73 + 79 = 152	867.49	1.015	864.90	1.062	862.28	1.099	859.62	1.115
75 + 77 = 152	867.54	1.023	865.08	1.071	862.58	1.107	860.05	1.122
77 + 75 = 152	867.16	1.024	864.82	1.072	862.45	1.109	860.05	1.122
79 + 73 = 152	866.34	1.016	864.13	1.064	861.89	1.101	859.62	1.115
71 + 79 = 150	875.80	0.906	873.13	0.942	870.42	0.965	867.68	0.969
73 + 77 = 150	876.09	0.915	873.54	0.948	870.96	0.967	868.35	0.966
75 + 75 = 150	875.92	0.923	873.51	0.955	871.06	0.970	868.58	0.965
77 + 73 = 150	875.31	0.931	873.02	0.962	870.70	0.974	868.35	0.966
79 + 71 = 150	874.25	0.937	872.09	0.969	869.90	0.980	867.68	0.969

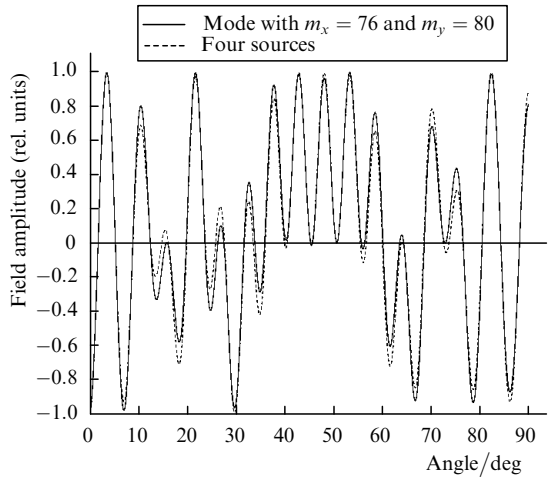

Figure 6. Amplitude radiation patterns of the 13×14-μm cavity and of four in-phase point sources of the same intensity located at the corners of a rectangle of the same size.

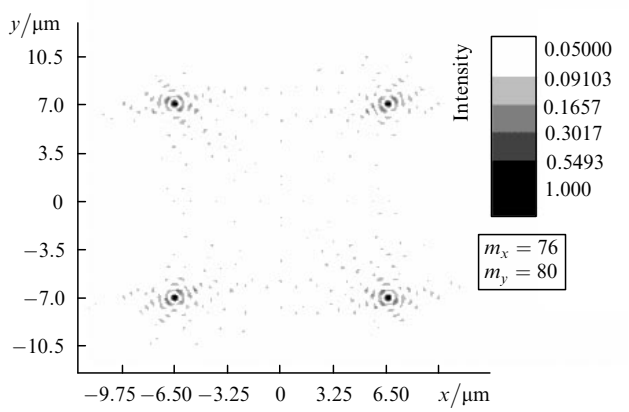

Figure 7. Shape of the function of sources reconstructed by the far-field radiation of the 13×14-μm cavity.

Thus, the analysis of radiation waves corresponding to the highest-Q modes of a rectangular cavity both in the far and near zones shows that they correspond to the wave emerging from the cavity corners. This completely corresponds to the experimental data obtained for output radiation of a semiconductor laser with a rectangular (four-sided) cavity.

5. Discussion and conclusions

Thus, the results of our paper lead to the following conclusions:

(i) Unlike a Fabry–Perot cavity, a rectangular cavity has a very dense system of nonequidistant modes, which cannot be in principle interpreted as modes of some 'effective' Fabry–Perot resonator or a ring laser. The intermode interval of a nearly square cavity can be arbitrarily small. For example, the minimal intermode distance for any mode pairs in the 13×13.1-μm cavity was smaller than 0.01 Å.

(ii) The Q factor of the modes related to the radiation loss is maximal for the TE modes propagating along the cavity diagonal, which is caused by the weaker exponential 'tails' of the filed for such modes. The Q factor for these modes can exceed 10^5, which corresponds to the reduced intracavity volume loss ~ 3 cm^{-1}.

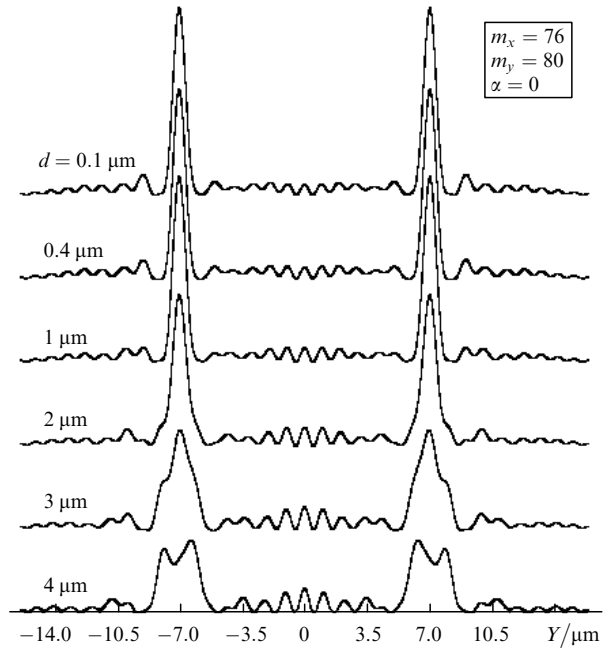

Figure 8. Microscopic images of the 13×14-μm cavity with the excited mode with indices 76 and 80. The positions of the object plane correspond to $\alpha = 0$ and $d = 0.1$, 0.4, 1, 2, 3, and 4 μm.

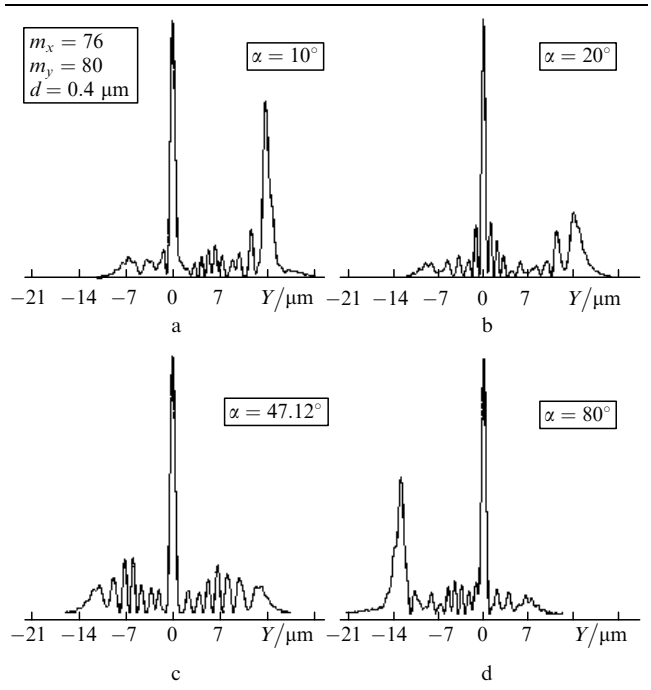

Figure 9. Microscopic images of the 13×14-μm cavity with the excited mode with indices 76 and 80. The positions of the object plane correspond to $d = 0.4$ μm and $\alpha = 10°$ (a) and 20° (b); the direction of the cavity diagonal correspond to 47.12° (c) and 80° (d).

(iii) The radiation field of a rectangular cavity can be interpreted as the field of four coherent point sources located at the cavity corners.

The results of our paper show that the analysis of the mode structure of the spectrum of a rectangular cavity performed in paper [9] in terms of a Fabry–Perot resonator is incorrect.

Note also that the determination of the laser radiation spectrum is a more complicate problem than the determination of intrinsic resonances. The matter is that analysis of a laser regime is a substantially nonlinear problem, in which not only the separation of mode resonances by the spectral amplification band of a medium should be considered, but also the saturation of this amplification by laser radiation. To determine which of the allowed cavity modes can be excited simultaneously, it is necessary to solve a problem of the gain saturation taking into account the spatial 'burning' of inversion by finding the self-consistent distribution of the field and carrier concentration. It seems that the surface recombination of carriers along the cavity boundaries also should be taken into account. These mechanisms determine the effective spatial overlaps of the field of an individual mode with inversion and, therefore, the effective amplification of this mode and its ability to be excited.

However, the calculation of the emission spectrum of a laser is beyond the scope of our paper. Here, we point out only that the presence or absence of equidistant or non-equidistant modes in the emission spectrum of a laser with a rectangular cavity does no allow one to make any conclusions about the value of the group refractive index, as has been made in paper [9].

Acknowledgements. This work was supported by the programs 'Quantum Nanostructures' of the Presidium of the Russian Academy of Sciences and 'Coherent Optical Radiation of Semiconductor Compounds and Structures' of the Department of Physical Sciences of the Russian Academy of Sciences, the Federal specific program 'Studies and Developments in the Priority Directions of the Development of the Scientific and Technological Complex of Russia in 2007–2012' (State Contract No. 02.513.11.3168), and Grant No. NSh-6055.2006.02 of the President of the Russian Federation for the Support of the Leading Scientific Schools.

References

1. Oraevsky A.N. *Kvantovaya Elektron.*, **32**, 377 (2002) [*Quantum Electron.*, **32**, 377 (2002)].
2. Braginsky V.B., Il'chenko V.S. *Dokl. Akad. Nauk SSSR*, **32**, 307 (1987).
3. Gorodetsky M.L., Savchenkov A.A., Ilchenko V.S. *Opt. Lett.*, **21**, 453 (1996).
4. Poon A.W., Courvoisier F., Chang R.K. *Opt. Lett.*, **26**, 632 (2001).
5. Guo W.H., Huang Y.Z., Lu Q.Y., Yu L.J. *IEEE J. Quantum Electron.*, **39**, 1563 (2003).
6. Guo W.H., Huang Y.Z., Lu Q.Y., Yu L.J. *IEEE Photon. Technol. Lett.*, **16**, 479 (2004).
7. Garrett C.G.B., Kaiser W., Bond W.L. *Phys. Rev.*, **124**, 1807 (1961).
8. Strakhov V.P. *Zh. Eksp. Teor. Fiz.*, **123**, 1276 (2003).
9. Strakhov V.P. *Zh. Eksp. Teor. Fiz.*, **126**, 469 (2006).
10. Adams M. *An Introduction to Optical Waveguides* (New York: Wiley, 1981; Moscow: Mir, 1984).
11. Landau L.D., Livshits E.M. *Electrodynamics of Continuous Media* (Oxford: Pergamon Press, 1984; Moscow: Nauka, 1982).
12. Born M., Wolf E. *Principles of Optics* (Oxford: Pergamon Press, 1969; Moscow: Nauka, 1973).